Int. J. Heat Mass Transfer. Vol. 36, No. 13, pp. 3201–3209, 1993
Printed in Great Britain

0017–9310/93 $6.00+0.00

Superadiabatic combustion in a porous medium

KATSUNORI HANAMURA
Department of Mechanical Engineering, Gifu University, 1-1 Yanagido, Gifu 501-11, Japan

RYOZO ECHIGO
Department of Mechanical Engineering, Tokyo Institute of Technology, 2-12-1 Ohokayama, Meguro-ku, Tokyo 152, Japan

and

SERGUEI A. ZHDANOK
Heat and Mass Transfer Institute, Byelorussian Academy of Science, 25 Podlesnaya, Minsk 220728, Belarus

(*Received* 6 *October* 1992 *and in final form* 3 *February* 1993)

Abstract—Superadiabatic combustion with reciprocating flow in a porous medium has been investigated through a numerical calculation. In this system, a combustible gas with an extremely low heat content flows into the porous medium, where the flow direction reverses regularly. By the reciprocating flow system, the combustion gas enthalpy is effectively regenerated into an enthalpy increase in the combustible gas through the porous medium, which provides heat storage. The results have revealed that the flame temperature in the porous medium is 13 times higher than the theoretical one of the ordinary flame in free space. The heating value of the combustible gas is about 65 kJ m^{-3}, which is equivalent to a temperature increase of only 50 K.

1. INTRODUCTION

RECENTLY, in the attempt to protect the global environment, demand has grown for the incineration of pollutants exhausted from various industries and methane in the ventilation air from mines and so on. These gases are usually diluted by a large amount of air and/or inert gases. As a result, the heating value is smaller than about 250 kJ m^{-3}, which is equivalent to the temperature increase of about 200 K. Therefore, a large amount of external energy must be supplied to burn these gases, as long as ordinary combustion technologies are utilized. However, if self-sustaining combustion is applied to burn these low heat content gases, all of the additional energy can be saved, and, further, it is possible to extract the energy from these dilute fuels. To this end, combustion augmentation has been proposed on the basis of the concept of excess enthalpy burning, in which heat is transmitted from hot combustion products to cold reactants through various heat transfer processes. Heat-recirculation systems, such as those involving convective heat exchange [1–3], thermal conduction through a flame in a porous plug [4, 5] and radiation transfer in a highly porous medium [6–9], have been shown to be effective over the past decade.

Of these systems, radiation-controlled combustion in the porous medium, which has been proposed by the present authors [6–9], shows the best combustion enhancement performance. In a previous study, the structure of the flame stabilized in the porous medium has been clarified through experiments and numerical calculations [7–9]. In the radiation-controlled flame, strong energy feedback by radiation through the reaction zone yields a flame temperature higher than the theoretical one. The same thermal structures have been obtained for combustion systems in a porous honeycomb body [10] and a fibrous porous radiant burner [11–13]. Further, the more detailed structure of the radiation-controlled flame has been investigated using multistep reaction kinetics [14].

Furthermore, as the porous medium, which has an infinite length along the flow direction, moves continuously in the direction opposite that of the gas flow, most of the combustion gas enthalpy can be stored by the porous medium. Then, the stored heat is transported to the preflame zone through the reaction zone to preheat the mixture. As a result, a superadiabatic system, in which there is hardly any outflow enthalpy, can be established in the porous medium. Similarly, when a mixture is introduced with reciprocating flow, superadiabatic combustion is also realized in the porous medium with a finite length. Recently, the latter system has been successfully applied to burning of the organic pollutants in exhaust air from paint spray boxes in car factories [15]. In that study, the mixture was introduced to a bed of silica gravel, where the flow direction through the bed was alternatively changed at regular intervals. The theoretical temperature increase of the mixture was only 20 K. In other words, in the porous medium, most of the combustion heat released from a high-quality fuel can be

NOMENCLATURE

A	frequency factor for combustion [s^{-1}]
A_s	specific surface area of a particle [$m^2\ m^{-3}$]
C_p	specific heat at constant pressure [kJ $kg^{-1}\ K^{-1}$]
C_s	specific heat of porous medium [kJ $kg^{-1}\ K^{-1}$]
D	diffusivity [$m^2\ s^{-1}$]
E	activation energy [kJ $kmol^{-1}$]
E_n	exponential integral function of nth order
E_a	dimensionless activation energy; equation (8)
H	dimensionless radiation flux; equation (8)
H_0	dimensionless combustion heat; equation (8) (dimensionless heating value for uniform heating)
h_0	combustion heat, $C_p(T_{th}-T_0)$ [kJ kg^{-1}] (heating value for uniform heating)
I_b	blackbody radiation intensity [W m^{-2}]
I_e, I_0	incident radiance, σT_0^4 [W m^{-2}]
Le	Lewis number, $\rho_g C_p D/\lambda_g$
M	dimensionless heat transfer coefficient between working gas and porous medium; equation (8)
N_r	conduction–radiation parameter; equation (8)
n_s	number density of particles [m^{-3}]
Pr	Prandtl number, $\rho_g \nu C_p/\lambda_g$
q_r	net radiation flux [W m^{-2}]
R	universal gas constant [kJ $kmol^{-1}\ K^{-1}$]
Re	Reynolds number, ux_c/ν
R_s	dimensionless frequency factor; equation (8)
r_c	thermal conductivity ratio; equation (8)
T	temperature [K]
T_{th}	theoretical flame temperature [K] (theoretical increase-temperature)
t	time [s]
t_c	half cycle [s]
u	gas velocity [m s^{-1}]
W	reaction rate [kg $m^{-3}\ s^{-1}$]
X	dimensionless coordinate; equation (8)
x	coordinate [m]
x_c	length of porous medium [m]
Y	product mole fraction.

Greek symbols

α_s	heat transfer coefficient around a particle [W $m^{-2}\ K^{-1}$]
β	dimensionless time; equation (8)
β_c	dimensionless half cycle
Γ	heat capacity ratio between two phases; equation (8)
η_c	combustion efficiency
κ	absorption coefficient [m^{-1}]
λ	thermal conductivity [W $m^{-1}\ K^{-1}$]
$\tilde{\mu}$	cosine
ν	kinematic viscosity [$m^2\ s^{-1}$]
ρ	density [kg m^{-3}]
σ	Stefan–Boltzmann constant, 5.67×10^{-8} W $m^{-2}\ K^{-4}$
τ	optical length, κx
τ_e	optical thickness of porous medium, κx_e.

Subscripts

b	blackbody
g	working gas
s	porous medium.

converted into other kinds of energies, such as electric or mechanical power and endothermic reaction heat in autothermic steam-reforming, where only the enthalpy equivalent to the temperature increase of 20 K is exhausted from the end of the porous medium. Consequently it is considered that the radiation-controlled combustion integrated with reciprocating flow in the porous medium is an epoch-making technology, which can be applied to most combustion systems.

In the present work, an analytical study on super-adiabatic combustion with reciprocating flow has been performed through a numerical calculation over a wide range of working parameters.

2. PHYSICAL MODEL

Figure 1 shows a schematic diagram of a one-dimensional physical model, where the geometrical and optical length of the porous medium are, respectively, x_c and τ_e. In the porous medium and gas-phase regions of $x_0 \leqslant x \leqslant 0$ and $x_c \leqslant x \leqslant x_{oe}$, a working gas flows uniformly with a velocity u. The flow direction is reversed at regular intervals t_c, which represents the

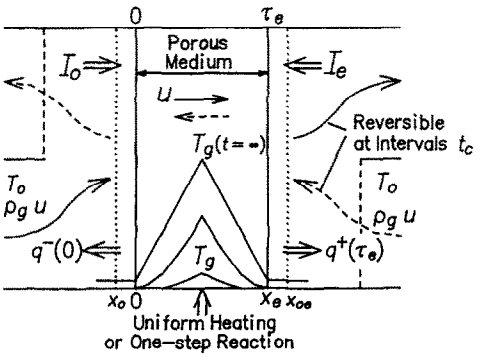

FIG. 1. Schematic diagram of physical model and schematic temperature profiles at each time step from $t = 0$ to ∞.

half cycle of the system. The entrance gas temperature T_o at $x = x_o$ (or $x = x_{oe}$) is 298 K. Two models are considered here for the heating: (I) uniform heating fixed at the middle of the porous medium, (II) combustion based on a one-step reaction with the Arrhenius rate expression. Both ends of the porous medium are exposed to black surfaces maintained at an ambient temperature T_o providing incident radiances I_o and I_e. On the other hand, there are radiant heat losses $q^-(0)$ and $q^+(\tau_e)$ outside the combustion system.

Most of the assumptions are identical to those of ordinary flame theory. Further, the additional assumptions for radiative transfer and the reaction system are as follows:

(1) the working gas is nonradiating,

(2) the porous medium consists of fine solid particles dispersed homogeneously,

(3) the porous medium is able to emit and absorb thermal radiation in local thermodynamic equilibrium,

(4) the combustion reaction for model (II) is described by an irreversible first-order isomerization (i.e. Reactant → Product),

(5) the porous medium is noncatalytic,

(6) the Lewis number is unity,

(7) the physical properties are constant.

3. BASIC EQUATIONS

With the use of the preceding assumptions, under the one-step reaction with the Arrhenius rate expression, the energy equations for both gas and solid phases and the conservation equation for product species are formulated, respectively, as follows:

$$C_p\rho_g\frac{\partial T_g}{\partial t}+C_p\rho_g u\frac{\partial T_g}{\partial x}=\lambda_g\frac{\partial^2 T_g}{\partial x^2}+h_o W-\alpha_s n_s A_s(T_g-T_s), \quad (1)$$

$$C_s\rho_s\frac{\partial T_s}{\partial t}=\lambda_s\frac{\partial^2 T_s}{\partial x^2}-\frac{\partial q_r}{\partial x}+\alpha_s n_s A_s(T_g-T_s), \quad (2)$$

$$\rho_g\frac{\partial Y}{\partial t}+\rho_g u\frac{\partial Y}{\partial x}=D\rho_g\frac{\partial^2 Y}{\partial x^2}+W. \quad (3)$$

The third term on the right-hand sides of equations (1) and (2) express the heat transfer between two phases. The reaction rate W is derived from the assumptions, as follows:

$$W=A\rho_g(1-Y)\exp(-E/RT_g). \quad (4)$$

The divergence of the radiation flux vector is evaluated from integration of the radiation intensity emitted from the other parts of the porous medium and represented for one-dimensional radiation, as follows:

$$\frac{\partial q_r(\tau)}{\partial x}=-2\pi\kappa[I_o E_2(\tau)+I_e E_2(\tau_e-\tau)-2I_b(\tau)+\int_0^{\tau_e} I_b(\tau')E_1(|\tau-\tau'|)\,d\tau'], \quad (5)$$

where $I_b(\tau)$ and $E_n(\tau)$ denote, respectively, the blackbody radiation intensity and the exponential integral function of the nth order, as follows:

$$I_b(\tau)=\frac{\sigma T_s^4}{\pi}, \quad E_n(\tau)=\int_0^1 \tilde{\mu}^{n-2}\exp(-\tau/\tilde{\mu})\,d\tilde{\mu}. \quad (6)$$

In the regions of $x_o \leqslant x \leqslant 0$ and $x_e \leqslant x \leqslant x_{oe}$, the heat release rate is assumed to be negligible since the temperature is extremely low.

On the other hand, under uniform heating, heat h_o is uniformly released within the limited region around the middle of the porous medium. Here, the conservation equation for product species Y is eliminated.

The boundary conditions are expressed as follows:

for the positive flow direction,

$$T=T_o, \quad Y=0 \quad \text{at} \quad x=x_o,$$
$$\partial T/\partial x=\partial Y/\partial x=0 \quad \text{at} \quad x=x_{oe};$$

for the negative flow direction,

$$T=T_o, \quad Y=0 \quad \text{at} \quad x=x_{oe},$$
$$\partial T/\partial x=\partial Y/\partial x=0 \quad \text{at} \quad x=x_o. \quad (7)$$

4. COMPUTATIONAL PROCEDURE

Basic equations were transformed into dimensionless forms and calculated using the finite difference method. In the numerical calculation, the flame position is not specified beforehand, but is decided as a result from the total energy balance in the combustion system. The principle dimensionless variables and parameters adopted here are as follows:

$$X=x/x_e, \quad \tau_e=\kappa x_e, \quad \beta=ut/x_e,$$
$$\beta_c=ut_c/x_e, \quad Re=ux_e/\nu, \quad Pr=\rho_g\nu C_p/\lambda,$$
$$\Gamma=\rho_s C_s/\rho_g C_p, \quad r_c=\lambda_s/\lambda_g, \quad H=q_r/4\sigma T_o^4,$$
$$H_o=h_o/C_p T_o=(T_{th}-T_o)/T_o, \quad Le=\rho_g C_p D/\lambda_g=1,$$
$$M=x_e^2\alpha_s n_s A_s/\lambda_g, \quad Nr=\kappa\lambda_g/4\sigma T_o^3,$$
$$E_a=E/RT_o, \quad R_s=Ax_e^2/\nu. \quad (8)$$

A spongelike porous material made of cordierite has, for example, a porosity of 87.5% (Bridgestone Corp. [16]). Then, the values of dimensionless parameters are approximately $\Gamma=300$, $r_c=1$, $M=6\times10^6$, $\tau_e=500$ and $N_r=5$, as $x_e=1$ m. Herein, the mean free path of radiation κ^{-1} is equal to the mean diameter of a pore of the porous medium, i.e. $\kappa^{-1}=2$ mm. The value of the specific surface area, i.e. the product of n_s and A_s, of the porous medium is approximately 3000 $m^2\ m^{-3}$. The heat transfer coefficient α_s was estimated from the heat transfer around a sphere, the diameter of which is equal to the mean diameter of the element forming the spongelike porous medium. Furthermore, as $u=1$ m s^{-1}, the value of Re is approximately 10 000 and β is equivalent to the time t in seconds.

On the other hand, the values of the frequency

factor and the activation energy were estimated from the evaluation of the burning velocity to be equal to measured values at equivalence ratios of $\phi = 0.53$ and 1.0, resulting in $A = 2.6 \times 10^8$ s^{-1} and $E = 130$ kJ mol^{-1}. Consequently, the dimensionless values of $R_s = 10^{12}$ and $E_a = 50$ are adopted for the standard calculation.

Furthermore, both lengths of the free space $x_o \leqslant x \leqslant 0$ and $x_e \leqslant x \leqslant x_{eo}$ are assumed to be one-twentieth of the thickness of the porous medium.

5. RESULTS AND DISCUSSION

5.1. *Superadiabatic system (uniform heating)*

Figure 1 shows the schematic profiles of the gas temperature at each time step from $t = 0$, where $T_g = T_s = T_o$, to $t = \infty$. Here, uniform heating occurs at the middle of the porous medium. The thickness of the heating zone is one-fiftieth of the length of the porous medium. A working gas introduced into the porous medium is, first, heated in the heating zone. Then, during the period when the hot gas passes through the porous medium, the gas temperature decreases almost to the ambient one T_o before reaching the downstream exit; i.e. the porous medium provides heat storage. On reversal, the cold working gas flows through the porous medium and becomes preheated before entering the heating zone. By the use of the reciprocating flow system, both gas and solid temperatures continue to increase up to the equilibrium point (at $t = \infty$), in which the amount of input heat is equal to that of the outflow enthalpy in a cycle; i.e. there is a steady state in this system.

Figure 2 shows the gas temperature profiles in the fully developed state. Herein, the value of dimensionless heating H_o is 0.2 (80 kJ m^{-3}), which is equivalent to a temperature increase of about 60 K. The flow direction reverses at regular intervals of $\beta_c = 5$ or 25. Both temperature profiles are shown only at $\beta = \beta_c$. In free space the maximum temperature is equal to the theoretical increase-temperature T_{th}/T_o of only 1.2, as depicted by the dashed line. However, in the porous medium the maximum gas temperature $T_{g,max}/T_o$ reaches the value of 4.5, as $\beta_c = 5$.

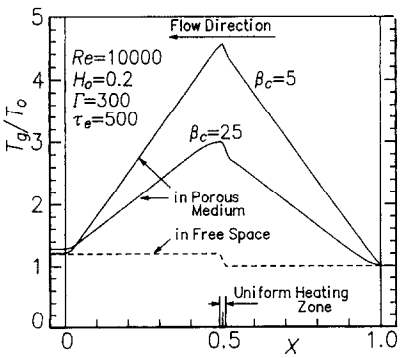

FIG. 2. Temperature distributions in porous medium with reciprocating flow and in free space; uniform heating.

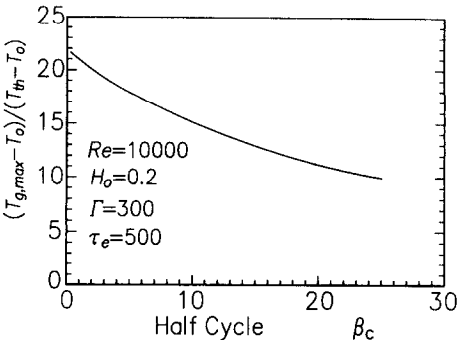

FIG. 3. Maximum temperature vs half cycle β_c; uniform heating.

In this system, after the flow direction has been reversed, the exit temperature increases gradually with time from $\beta = 0$ to β_c. Therefore, it is important to change the flow direction before the exit temperature becomes too high (Fig. 2). Consequently, the maximum temperature increases with decreasing β_c as shown in Fig. 3. Here, under the condition of $\beta_c = 0.3$, the maximum temperature $T_{g,max} - T_o$ in the porous medium exceeds the theoretical temperature $T_{th} - T_o$ by a factor of about 22.

The same temperature profiles as shown in Fig. 2 are obtained, as the solid phase releases heat, as in an electric heater.

5.2. *Superadiabatic combustion in porous medium (Arrhenius rate expression)*

5.2.1. *Transient behavior with respect to time.* Using the temperature profile in Fig. 2 as an initial condition, we can obtain the superadiabatic flames based on the Arrhenius reaction rate. Figures 4(a)–(e) show the profiles of the gas and solid temperatures T_g, T_s, the product mole fraction Y and the reaction rate RR at each time step from $\beta = 0$ to $\beta = \beta_c = 5$, where $H_o = 0.3$. After the flow direction has been reversed at time $\beta = 0$, the reaction rate RR decreases since the combustion product flows into the reaction zone (Figs. 4(a) and (b)). With time, since the fresh reactant reaches the high temperature region, the combustion reaction starts to occur around $X = 0.3$ (Fig. 4(c)) to a significant extent. On the other hand, the reaction around $X = 0.7$ is almost extinguished (Fig. 4(c) and (d)). That is, in response to the flow direction, two exothermic reaction zones are alternatively yielded at a distance of X_{RR} (Fig. 4(e)). Consequently, the temperature profile becomes trapezoidal provided that no heat extraction exists in the system.

5.2.2. *Controllable range of half cycle and Reynolds number.* Figure 5 shows the profiles of the gas temperature T_g and the reaction rate RR under the conditions of a half cycle β_c of 5, 15 and 25. These profiles are shown only at $\beta = \beta_c$. The exit temperature at $\beta = \beta_c$ increases with β_c. However, the amount of outflow enthalpy should be equal to that of input heat in the steady state. To this end, the flame has to

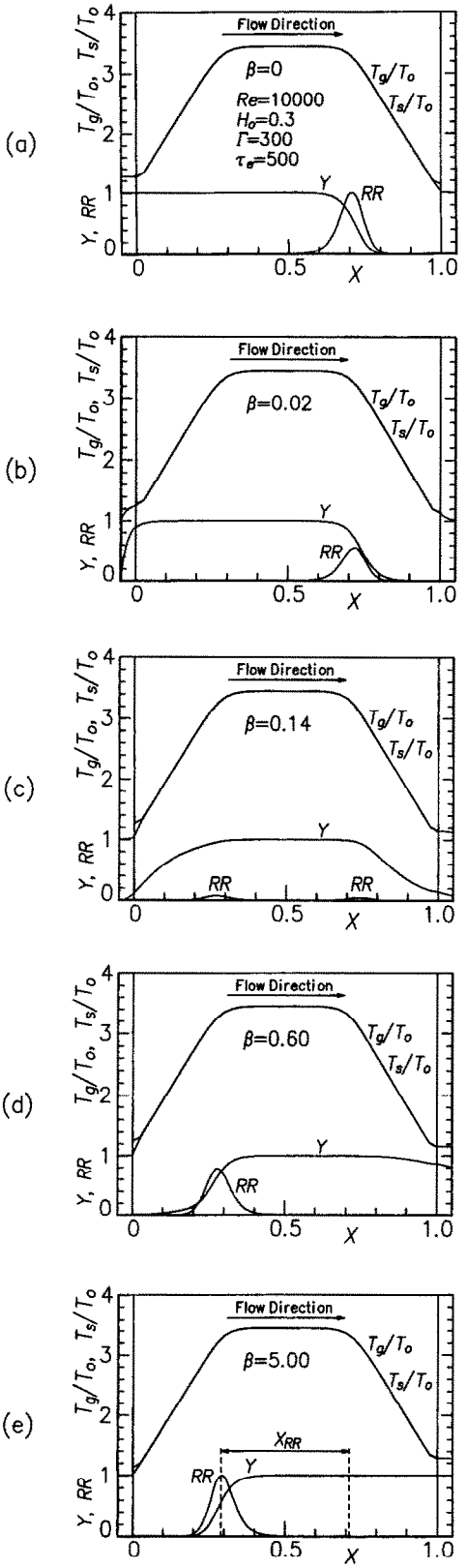

FIG. 4. Combustion with reciprocating flow in porous medium; profiles of gas and solid temperatures T_g/T_o, T_s/T_o, product mole fraction Y and reaction rate RR at each time step: (a) $\beta = 0$; (b) $\beta = 0.02$; (c) $\beta = 0.14$; (d) $\beta = 0.6$; (e) $\beta = \beta_c = 5.0$.

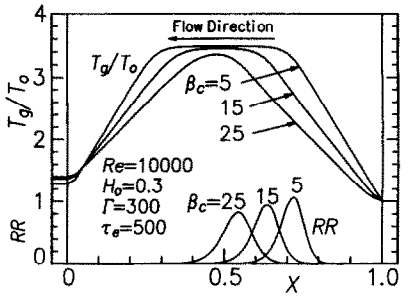

FIG. 5. Profiles of gas temperature T_g/T_o and reaction rate RR for half cycle β_c of 5, 15 and 25.

move deep into the porous medium, which creates a reduction in the temperature gradient around the exit. As a result, the increase rate of the exit temperature decreases with respect to time from $\beta = 0$ to β_c as shown in Fig. 6. Consequently, over a wide range of β_c, the maximum temperature is almost maintained at a constant as shown in Fig. 7, while for fixed heating, a reduction in the maximum temperature results in a decrease in the temperature gradient around the exit (Fig. 2).

On further increase in β_c from 25.5 to 26, the flame propagates in the downstream direction over the cross

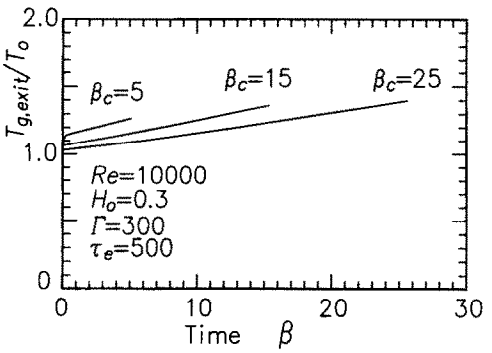

FIG. 6. Increase rate of the exit temperature $T_{g,exit}/T_o$ in a half cycle from $\beta = 0$ to β_c.

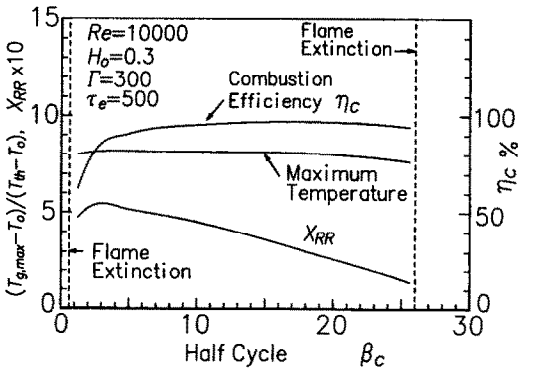

FIG. 7. Controllable range of half cycle β_c; maximum temperature, combustion efficiency η_c and distance between two reaction zones X_{RR} vs β_c.

section at $X = 0.5$, behind which the temperature decreases sharply. Therefore, combustion cannot be sustained in the porous medium as shown in Fig. 7. The extinction limit for β_c is extended by the increase in the heat capacity ratio Γ between the porous medium and flowing gas.

In this combustion system, the reactant, which remains in the region from the entrance to the flame location, flows out as the flow direction reverses, as shown in Fig. 4. As a result, in the range of a short half cycle, the combustion efficiency η_c decreases drastically with decreasing β_c as shown in Fig. 7. Finally, the flame disappears under the condition of $\beta_c < 0.6$. This is because the flow direction changes before the reactant reaches the hgh-temperature region and burns.

Similarly, upper and lower extinction limits exist for the higher and lower values of Reynolds number Re, respectively. However, as shown in Fig. 8, the flame is stabilized in the porous medium over a wide range of Re from 2000 to 53 000, where $\beta_c = 2.5$. With increasing Re, the ratio of the reaction rate to the flow velocity, i.e. R_s/Re, decreases, which results in the rise of the maximum temperature as illustrated in 5.2.4. As a result, in order to equalize the amount of outflow enthalpy to that of input heat, the flame automatically moves deep into the porous medium as mentioned above; thus, the distance between two reaction zones X_{RR} decreases.

5.2.3. *The effect of physical properties of porous medium.* Parameters, such as optical thickness τ_c, thermal conductivity ratio r_c, heat capacity ratio Γ and heat transfer coefficient between two phases M, are determined from the physical properties of the porous medium.

Figures 9(a) and (b) show the profiles of the temperatures T_g, T_s, the reaction rate RR, and the net radiation flux H under the conditions of the optical thickness τ_c of 0, 20, 50 and 500. As considered here, if the absorption coefficient κ varies, the conduction–radiation parameter increases in proportion to τ_c, i.e. $N_r = 0, 0.2, 0.5$ and 5, respectively. Under the optically

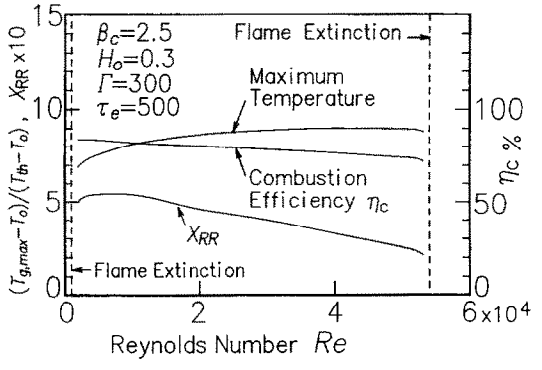

FIG. 8. Controllable range of Reynolds number Re; maximum temperature, combustion efficiency η_c and distance between two reaction zones X_{RR} vs Re.

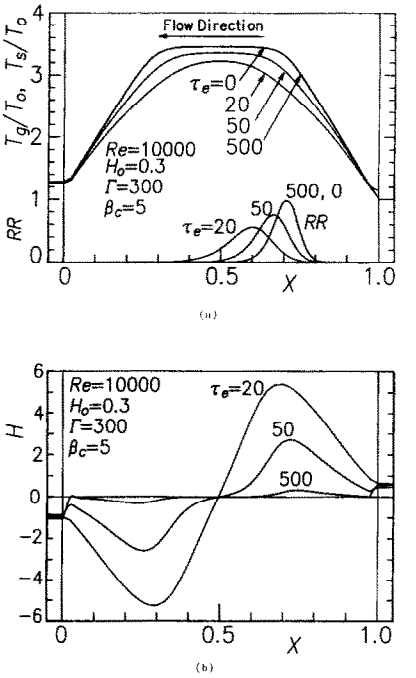

FIG. 9. (a) Profiles of gas temperature T_g/T_o and reaction rate RR for optical thickness τ_c of 0, 20, 50 and 500. (b) Radiation flux profiles in porous medium.

thick condition of $\tau_c = 500$, the absolute value of the net radiation flux is very small throughout the region of the porous medium. This is because the radiation intensity is attenuated in a short distance. As a result, the temperature profile for $\tau_c = 500$ is much the same as that for $\tau_c = 0$.

The net radiation flux around the reaction zone increases with decreasing τ_c. This indicates that a larger amount of radiant energy is fed back in the upstream direction through the reaction zone, yielding excess enthalpy burning [7–9]. However, to prevent an increase in the radiant heat loss outside the porous medium, the reaction zone must move deep into the porous medium. Therefore, as $\tau_c < 17$, the flame is no longer sustained in the porous medium as shown in Fig. 10.

Similarly, the flame disappears under the condition of $r_c > 75$, $\Gamma < 66$ or $M < 6.2 \times 10^5$ as shown in Figs. 11, 12 and 13, respectively. This is because the porous medium cannot provide adequate heat storage.

5.2.4. *The effect of reaction rate constant.* In the combustion with reciprocating flow in the porous medium, the maximum temperature is not so highly dependent on β_c, Re, τ_c, r_c, Γ and M. However, as shown in Figs. 14 and 15, the maximum temperature becomes higher in proportion to the activation energy E_a. On the other hand, with a decrease in frequency factor R_c, the maximum temperature rises as shown in Fig. 16. This is because, under a high activation energy or low frequency factor, the combustion reaction proceeds only in the high temperature region.

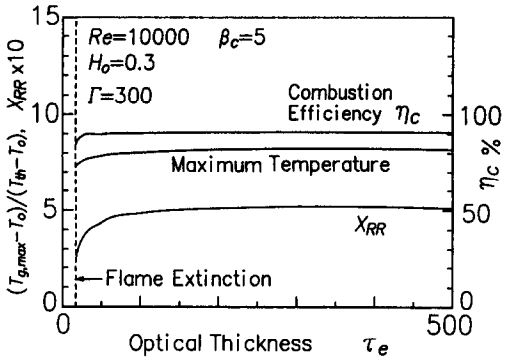

FIG. 10. Maximum temperature, combustion efficiency η_c and distance between two reaction zones X_{RR} vs optical thickness τ_e.

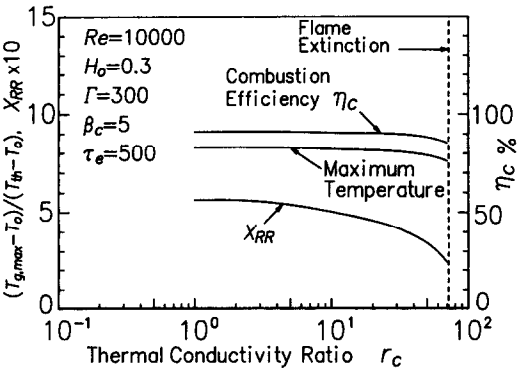

FIG. 11. Maximum temperature, combustion efficiency η_c and distance between two reaction zones X_{RR} vs thermal conductivity ratio r_c.

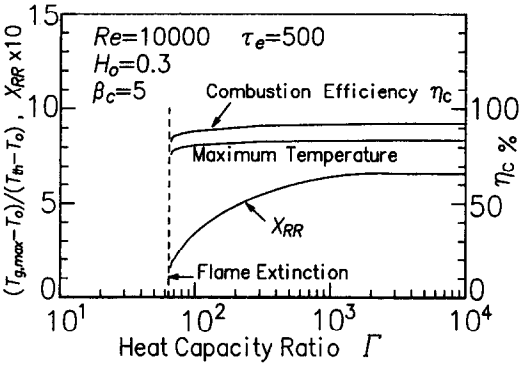

FIG. 12. Maximum temperature, combustion efficiency η_c and distance between two reaction zones X_{RR} vs heat capacity ratio Γ.

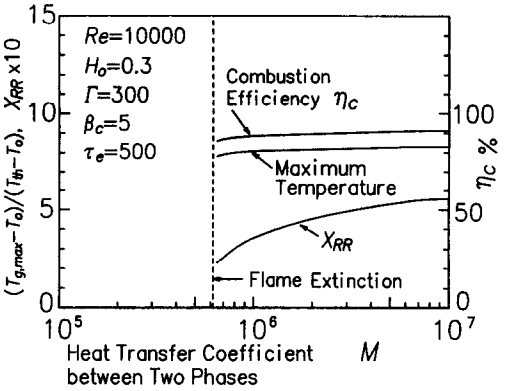

FIG. 13. Maximum temperature, combustion efficiency η_c and distance between two reaction zones X_{RR} vs heat transfer coefficient between two phases M.

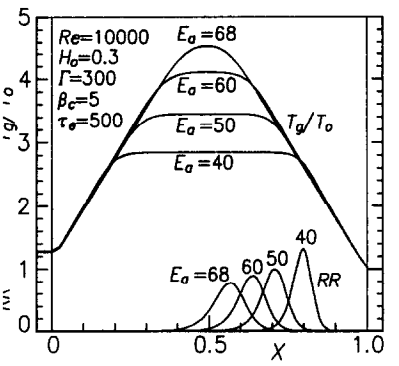

FIG. 14. Profiles of temperature T_g/T_o and reaction rate RR for activation energy E_a of 40, 50, 60 and 68.

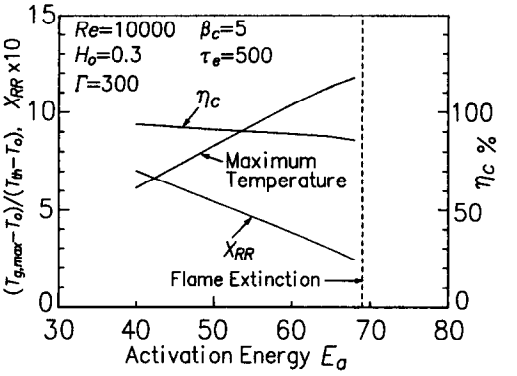

FIG. 15. Maximum temperature, combustion efficiency η_c and distance between two reaction zones X_{RR} vs activation energy E_a.

Here, the maximum temperature has to rise to the high ignition point. As a result, with increasing E_a, the flame is stabilized further from the entrance of the porous medium as shown in Fig. 14.

5.2.5. *Combustion augmentation for extremely low heat content gases.* Figure 17 shows the profiles of the gas temperature T_g and the reaction rate RR under the conditions of the combustion heat H_o of 0.17, 0.2, 0.3 and 0.4. With increasing H_o from 0.2 to 0.4, the maximum temperature $T_{g,max}/T_o$ increases with the difference between the values of H_o. This result implies that the maximum amount of heat, which can be transmitted from the combustion gas to the mixture, is recirculated by the reciprocating flow system in the

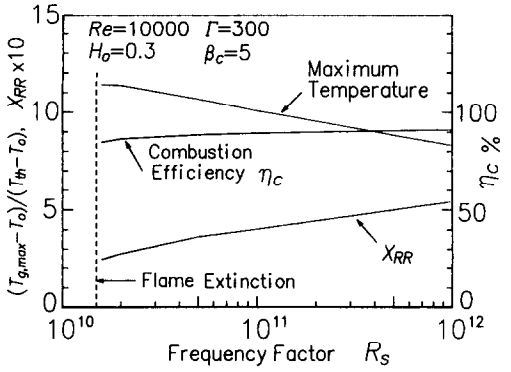

FIG. 16. Maximum temperature, combustion efficiency η_c and distance between two reaction zones X_{RR} vs frequency factor R_s.

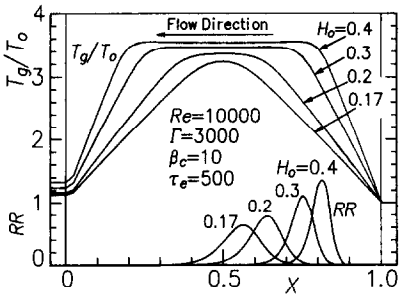

FIG. 17. Superadiabatic combustion for extremely low heat content gases.

porous medium. Further, since the amount of input heat increases with H_0, the reaction zone moves toward the end of the porous medium to increase the outflow enthalpy, i.e. to raise the temperature gradient around the exit.

On further decrease in H_0 from 0.17 to 0.16, the flame propagates further in the flow direction over the cross section at $X = 0.5$, behind which the temperature decreases sharply; since the temperature profile has an isosceles-triangle shape. As a result, a larger amount of unburnt gas flows out, which results in the flame extinction. Consequently, in the combustion

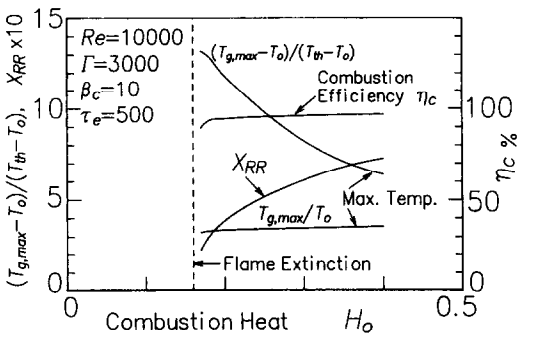

FIG. 18. Maximum temperature and combustion efficiency η_c vs combustion heat H_0.

with reciprocating flow in the porous medium, the broader plateau maintained at the maximum temperature indicates a higher potential for the extension of the flammable limit. As shown in Fig. 18, the maximum temperature $T_{g,max} - T_0$ for $H_0 = 0.17$ is 13 times higher than the theoretical temperature increase $T_{th} - T_0$. The heating value is 65 kJ m^{-3}, which is equivalent to the temperature increase of only 50 K.

6. CONCLUSIONS

Numerical analysis has been performed on superadiabatic combustion with reciprocating flow in a porous medium, with the rigorous treatment for radiation transfer, on the basis of two simplified heating models.

In uniform heating occurring at the middle of the porous medium, the temperature profile has an isosceles-triangle shape. The maximum temperature becomes higher with decreasing length of the half cycle, at which the flow direction is reversed regularly.

On the other hand, as the reaction rate is based on the Arrhenius rate expression, the temperature profile becomes trapezoidal. In response to the flow direction, two reaction zones are alternatively yielded at a distance of the length of the plateau maintained at the maximum temperature. The maximum temperature is determined almost solely from the reaction rate constant. On the other hand, the position of the reaction zone is strongly dependent on parameters, such as the half cycle, Reynolds number, optical thickness, conductivity ratio, heat capacity ratio and heat transfer coefficient between two phases. Furthermore, the flame disappears as the reaction zone moves deep into the porous medium over the cross section of the middle; concurrently, the temperature profile changes from the trapezoid to the isosceles-triangle shape.

The most striking feature is that the maximum temperature in this combustion system exceeds the theoretical one by a factor of about 13. The heating value of the mixture is only about 65 kJ m^{-3}.

REFERENCES

1. F. J. Weinberg, Combustion temperature: the future?, *Nature* **233**, 239–241 (1971).
2. A. R. Jones, S. A. Lloyd and F. J. Weinberg, Combustion in heat exchangers, *Proc. R. Soc. Lond. A.* **360**, 97–115 (1978).
3. T. Kawamura, K. Asato and T. Hayashi, Combustion of extra lean gaseous fuels by a burner with a heat exchanger, *Proc. ASME–JSME Thermal Engng Joint Conf.*, Honolulu, Vol. 4, pp. 93–98 (1983).
4. T. Takeno, K. Sato and K. Hase, A theoretical study on an excess enthalpy flame, *Eighteenth Symp. (Int.) on Combustion*, pp. 465–472. The Combustion Institute (1981).
5. Y. Kotani, H. F. Behbahani and T. Takeno, An excess enthalpy flame combustor for extended flow ranges, *Twentieth Symp. (Int.) on Combustion*, pp. 2025–2033. The Combustion Institute (1984).
6. R. Echigo, M. Kurusu, K. Ichimiya and Y. Toshizawa, Combustion augmentation of extremely low calorific gases (application of the effective energy conversion

method from gas enthalpy to thermal radiation), *Proc. ASME–JSME Thermal Engng Joint Conf.*, Honolulu, Vol. 4, pp. 99–104 (1983).
7. R. Echigo, Y. Yoshizawa, K. Hanamura and T. Tomimura, Analytical and experimental studies on radiative propagation in porous media with internal heat generation, *Proc. 8th Int. Heat Transfer Conf.*, San Francisco, Vol. 2, pp. 827–832 (1986).
8. Y. Yoshizawa, R. Echigo and K. Sasaki, Analytical study on the structure of radiation controlled flame, *Int. J. Heat Mass Transfer* **31**, 311–319 (1988).
9. K. Hanamura, Y. Yoshizawa and R. Echigo, Analytical study on the structure of radiation controlled flame in a highly porous medium, *Joint Int. Conf. Australia/New Zealand and Japanese Sections*, pp. 251–253. The Combustion Institute (1989).
10. D. K. Min and H. D. Shin, Laminar premixed flame stabilized inside a honeycomb ceramic, *Int. J. Heat Mass Transfer* **34**, 341–355 (1991).
11. K. Hanamura and R. Echigo, An analysis of flame stabilization mechanism in radiation burners, *Wärme- und Stoffübertragung* **26**, 377–383 (1991).
12. S. B. Sathe, R. E. Peck and T. W. Tong, A numerical analysis of heat transfer and combustion in porous radiant burners, *Int. J. Heat Mass Transfer* **33**, 1331–1338 (1990).
13. T. W. Tong, S. B. Sathe and R. E. Peck, Improving the performance of porous radiant burners through use of sub-micron size fibers, *Int. J. Heat Mass Transfer* **33**, 1339–1346 (1990).
14. P. Hsu, J. R. Howell and R. D. Matthews, A numerical investigation of premixed combustion within porous inert media, *Proc. ASME–JSME Thermal Engng Joint Conf.*, Reno, Vol. 4, pp. 225–231 (1991).
15. Commercial report, A new method of destroying organic pollutants in exhaust air, ADTEC Co., Ltd. (1990).
16. Technical report No. 1, Ceramic foam, Bridgestone Corp. (1986).